Sensors and Actuators A 321 (2021) 112416

Contents lists available at ScienceDirect

Sensors and Actuators A: Physical

journal homepage: www.elsevier.com/locate/sna

Position and force sensing using strain gauges integrated into piezoelectric bender electrodes

Rudolf Seethaler[a,*], Sepehr Zarif Mansour[a], Michael G. Ruppert[b], Andrew J. Fleming[b]

[a] University of British Columbia, Kelowna, BC V1V1H9, Canada
[b] University of Newcastle, Callaghan, NSW 2308, Australia

ARTICLE INFO

Article history:
Received 14 July 2020
Received in revised form 7 October 2020
Accepted 1 November 2020
Available online 7 November 2020

Keywords:
Piezoelectric bender
Position sensing
Force sensing

ABSTRACT

This article derives design guidelines for integrating strain gauges into the electrodes of piezoelectric bending actuators. The proposed sensor can estimate the actuator tip displacement in response to an applied voltage and an external applied tip force. The actuator load force is also estimated with an accuracy of 8% full scale by approximating the actuator response with a linear model. The applications of this work include micro-grippers and pneumatic valves, which both require the measurement of deflection and load force. At present, this is achieved by external sensors. However, this work shows that these functions can be integrated into the actuator electrodes.

1. Introduction

Among piezoelectric actuators, benders find the widest application in industrial applications due to their low cost, high reliability, and large displacement. One ubiquitous application for piezoelectric benders are buzzers in alarm devices, and timers. However, benders also find applications in more exotic applications such as braille heads [1]. A large application often overlooked are warp knitting machines that dominate the world's clothing fabric industry. These machines have been using piezoelectric bending actuators for moving their needles since the 1990s [2]. Other applications include fiber optic switches [3], or positioning of hard drive heads [4]. Recently, piezoelectric benders have also been integrated into pneumatic proportional control valves in applications such as mobile ventilators, oxygen therapy, dialysis machines, or pneumatic surgical tools [5]. Micro-scale benders also find applications in atomic force microscopy (AFM), where they constitute the key component to measuring features of samples with nanometer resolution [6].

Many piezoelectric actuators achieve adequate control performance with voltage feedforward control strategies [7,8], charge amplifiers [9,10], or position self sensing [11–13]. However, applications with stringent requirements for high accuracy, low drift, and robustness to disturbance forces require dedicated position, or force sensors.

Strain gauges have long been used for estimating displacement or force in piezoelectric manipulation systems. However they usually are not integrated into the actuator electrodes and they typically do not simultaneously measure displacement or force. A multidimensional piezoresistive force sensor for a micromanipulation system without position sensing is introduced in [14]. The flexure based microgripper driven by a stack actuator in [15] also measures gripping force using strain gauges but it lacks position feedback. The microgripper introduced in [16] uses a stack actuator to drive a flexure based gripper that is able to decouple strains due to gripper position and force. Thus, this design enables the use of strain gauges for independent measurement of gripper position and force. However this requires a complicated and large flexure design. Unfortunately, the sensing systems above only show static calibration curves or no comparison with reference sensors at all. This makes a detailed comparison of sensing performance difficult.

Integrating feedback sensors into the bender electrodes is an attractive low cost strategy for reducing the space requirements of the sensing elements. This is typically achieved by separating the electrodes into an actuation and sensing region using either etching or laser cutting. An early example of a piezoelectric sensor that is laser cut into bender electrodes is shown in Ref. [17]. The obtained piezoelectric sensor voltage is a function of both displacement and tip force. A linear model is used to decouple the two measurements using the voltage on the actuating portion of the electrodes as the second measurement. This technique, even though elegant, has two drawbacks. First, DC measurements are not possible, since the sensing voltage is piezoelectric in nature and

* Corresponding author.
E-mail address: rudolf.seethaler@ubc.ca (A.J. Fleming).

https://doi.org/10.1016/j.sna.2020.112416

suffers from charge leakage. Second, the accuracy of the measurement is limited by the linear decoupling operator that neglects all nonlinear effects such as hysteresis and creep. Integrated capacitive and inductive sensors have been proposed as position feedback signals for pneumatic valves in Ref. [18]. However, considerations such as accuracy, cost, and size have limited their commercial success. Active cantilevers with integrated piezoelectric displacement sensing on the chip level have also been applied to single frequency AFM [19] multi-frequency AFM [20] and single-chip AFM implementations [21]. However, simultaneous force and position sensing has not been shown for integrated AFM sensors.

An alternative to etching out portions of the active piezoelectric electrode layers of a bender in order to create sensing elements is sandwiching an additional piezoelectric sensing layer between two piezoelectric actuation layers [22]. This approach suffers from the same two drawbacks as [17]: poor low frequency performance due to charge leakage and limited sensing accuracy due to piezoelectric nonlinearities such as hysteresis and creep.

Recently, resistive strain gauges have been integrated along the length of bender electrodes leading to a simple and cost effective way to determine tip displacement [23] of micro benders. This technique avoids the lower frequency cutoff of piezoelectric sensors shown in [17]. However, the gauge factor between strain and displacement differs for an applied electric field and for an applied tip force due to the different bending curvatures of the two excitation modes. This essentially limits the strain based displacement measurement in [23] to applications with small forces at the tip of the bender. Similar to [17], one could augment this measurement with the bender driving voltage to extract both force and displacement. However, this requires detailed hysteresis modeling to achieve accurate position and force measurements.

In this article, we present a new methodology for designing the geometry of resistive strain gauges integrated into bender electrodes. The proposed geometry provides identical gauge factors between strain and tip deflection for bender actuating voltages and for tip forces. This overcomes the requirement for small tip forces observed in [23]. Also like [23], the resistive strain measurement does not suffer from poor low frequency performance observed in [17]. In addition, this article suggests a linear model for estimating tip forces from measurements of tip displacement and bender driving voltage. This force estimate is useful in applications such as piezoelectric grippers with force feedback, or fluid control valves. The remainder of this article is structured as follows: In Section 2, the proposed strain gauge geometry required for measuring tip displacements in the presence of significant tip forces is derived. Section 2.3 outlines a linear force model for estimating tip force from measurement of tip displacement and actuation voltage. Section 2.2 describes the importance of selecting the correct bridge circuit configuration in order to maximize the bandwidth of the integrated sensor-actuator. In Section 3, the quasi static performance of the integrated sensors are experimentally verified in response to applied voltages and external forces. Finally, conclusions are provided in Section 4.

2. Piezoelectric bender design

A bimorph T220-A4BR-2513XB piezoelectric bending actuator from Piezo systems with material and geometry data detailed in Table 1 is utilized in this work. Fig. 1 shows a schematic of such a Y-poled bimorph piezoelectric bender. The cantilever bender is clamped at its base and is free to move at its tip. The unclamped portion of the bender has a length of L. The bender consists of two piezoelectric layers (PZT 5A) which are separated by a grounded center electrode (Brass) and sandwiched between two outer electrodes (Nickel). The tip displacement and tip force are labeled Z and F respectively. The bender's deflection is a result of two input sources: The applied tip force F and the actuating voltage V applied to the outside bender electrodes.

Table 1
Bender specifications.

Parameter	Value
PZT material	PZT 5A
Center electrode material	Brass
Bender length L_0	63.5 mm
Bender width W	31.75 mm
Bender thickness t	0.51 mm
PZT thickness	0.19 mm
Center electrode thickness	0.13 mm
Spring constant k	0.388 N/mm
Resonant frequency f_0	88 Hz
Unclamped bender length L	57 mm
Strain gauge connector location x_1	0 mm
Strain gauge end location x_2	38 mm

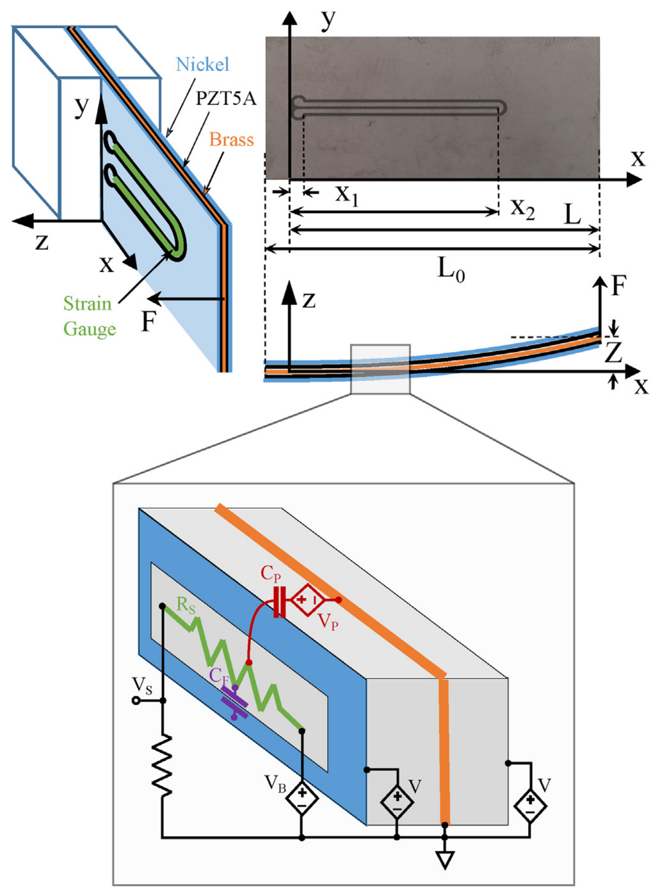

Fig. 1. Bender geometry with strain gauge embedded into outside electrodes. Strain gauge length is adjusted to achieve identical sensitivity between strain and displacement for both force and voltage excitation.

Two resistive strain gauges were factory laser cut into the outside electrodes according to Eq. (12) and electrically isolated from the rest of the high voltage driving electrodes. The bender is rigidly clamped up to the strain gauge connectors at x_1 and extend to the position x_2. In the following subsection, this position is derived such that a tip force and actuation voltage yield equal strain sensitivity at the strain gauge.

2.1. Sensor geometry

The strain sensor geometry proposed in this section provides a strain response linearly proportional to tip displacement. The displacement can be induced by an actuating voltage or a tip force. Using Bernoulli-Euler Beam theory, the former results in a linearly increasing bending moment towards the clamped base of the bender, whereas the latter creates a uniform bending moment M_p along the length of the bender [24].

$$M = M_p + F(L - x), \tag{1}$$

where M is the bending moment along the length of the bender. Since the bending moment of a beam is the second derivative deflection, the bender's deflection along its length is cubic for tip forces, and parabolic for applied voltages. This leads to the conclusion that for the same tip deflection, the strain along the length of the bender will also differ for tip forces and actuating voltages.

The strain gauges need to measure tip deflection due to actuating voltages and tip forces. This requires identical sensitivity between strain and tip displacement for voltage and force excitation:

$$\frac{dS}{dZ} = \frac{dS}{dF}\frac{dF}{dZ} = \frac{dS}{dM_p}\frac{dM_p}{dZ} \tag{2}$$

where, S is the average strain along the length of the strain gauges and Z is the tip deflection of the bender. The following paragraphs will first derive the terms in Eq. (2), before obtaining design equations for x_1 and x_2.

The tip deflection Z in Eq. (2) can either be obtained by integrating the bending moment in Eq. (1) twice or by super-positioning standard beam deflection formulas tabulated in [24]:

$$Z = F\left(\frac{L^3}{3EI} + \frac{L}{\gamma}\right) + M_p\frac{L^2}{2EI}, \tag{3}$$

where E is the Young's modulus, I is the second moment of area, and γ is the torsional stiffness of the clamping at the base of the bender. The sensitivity of tip displacement Z to a tip force F and a uniform bending moment M_p generated by a voltage on the actuating electrodes are given by:

$$\frac{dZ}{dF} = \frac{L^3}{3EI} + \frac{L}{\gamma} \tag{4}$$

$$\frac{dZ}{dM_p} = \frac{L^2}{2EI} \tag{5}$$

Local strain ε in the outside bender electrode is related to the bending moment by Ref. [24]:

$$\varepsilon = \frac{Mt}{2EI}, \tag{6}$$

where t is the thickness of the bender. However, a strain gauge measures the average strain S along its length:

$$S = \frac{\int_{x_1}^{x_2} \varepsilon dx}{(x_2 - x_1)} = \frac{t}{2EI}\left[M_p + F\left(L - \frac{x_1 + x_2}{2}\right)\right] \tag{7}$$

The derivatives of average strain S with respect to F and M_p yield the missing terms in Eq. (2):

$$\frac{dS}{dF} = \frac{t}{2EI}\left(L - \frac{x_2 + x_1}{2}\right) \tag{8}$$

$$\frac{dS}{dM_p} = \frac{t}{2EI} \tag{9}$$

Substituting Eqs. (4), (5), (8), and (9) into Eq. (2) yields a relationship for selecting the starting and end positions of the strain gauge along the length of the bender:

$$x_2 + x_1 = \frac{2L}{3} - \frac{4EI}{L\gamma} \tag{10}$$

Eq. (10) indicates that there are many feasible combinations of x_1 and x_2. For the special case of a rigidly clamped base, the strain sensor needs to be symmetrical around the 1/3 point of the bender:

$$\frac{x_2 + x_1}{2}\Big|_{\gamma=\infty} = \frac{L}{3} \tag{11}$$

A similar finding was shown for a capacitive strain sensor using numerical simulations [18]. To minimize the resistance variation of the strain gauge caused by manufacturing tolerances, one would maximize the length of the strain gauges. This leads to another special case, where the strain gauge starts at the rigidly clamped base:

$$x_2|_{x_1=0,\gamma=\infty} = \frac{2L}{3} \tag{12}$$

In practice, it can be difficult to achieve rigid clamping with $\gamma = \infty$. Non rigid clamping requires shorter strain gauges:

$$x_2|_{x_1=0} = \frac{2L}{3} - \frac{4EI}{L\gamma} \tag{13}$$

In summary, the ideal strain gauge configuration starts at the base of a rigidly clamped bender and spans two thirds of the length of the bender. For an elastic clamping of the bender at its base, the length of the bender needs to be reduced using the relationship shown in Eq. (13).

2.2. Strain gauge instrumentation

Even though the electrode configuration in Fig. 1 minimizes capacitive feedthrough from the driving electrodes [23], there is still some capacitive coupling between the strain gauges and the actuating electrodes that is modeled by a coupling capacitance C_F. In addition, the piezoelectric layers underneath the strain gauges will induce a piezoelectric voltage V_P that is coupled into the strain gauges through the coupling capacitance C_P. Both of these couplings will lead to high frequency feedthrough that can be minimized by properly configuring the Wheatstone half bridge used for converting strains to measurable voltages.

For opposing resistance changes the two half bridge configurations depicted in Fig. 2 are possible [25]. Both configurations are biased with a voltage V_B and the change in strain S, is measured as the differential bridge voltage V_S. The two configurations differ in where the active strain resistors R_{s1} and R_{s2} are placed within the bridge circuit and balanced by bridge completion resistors R_{B1} and R_{B2}. High frequency feedthrough from C_{F1} and C_{F2} is subtracted in configuration(a), but not in configuration(b). The same applies to the induced piezoelectric voltage coupled into the bridge circuit through C_{P1} and C_{P2}. Since both of these feedthrough signals are typically almost identical between the two outer electrodes, configuration(a) provides much lower feedthrough than configuration(b).

This is confirmed by a frequency response measurement shown in Fig. 3 where tip displacement Z and bridge voltage V_S is measured with a Polytech PSV-Z-040 frequency analyzer. The low frequency gain of −40 dB indicates a displacement of 1 mm for an actuating voltage of 100 V. The strain responses of the two bridge configurations are scaled to provide the same low frequency gain as the tip displacement. All three responses show identical resonance peaks at 78 Hz and 135 Hz. However, capacitive coupling into the strain signals from the driving voltage and the induced piezoelectric voltage leads to significant high frequency feedthrough. Since the feedthrough components from V and V_P are subtracted between the outside electrodes in configuration(a) but not in configuration(b), the corner frequency of V_S is much higher in configuration(a). Thus, the experiments in the remaining sections of this article are carried out with bridge configuration(a). This configuration displays a bandwidth of 44Hz as defined by −45 deg phase angle of the

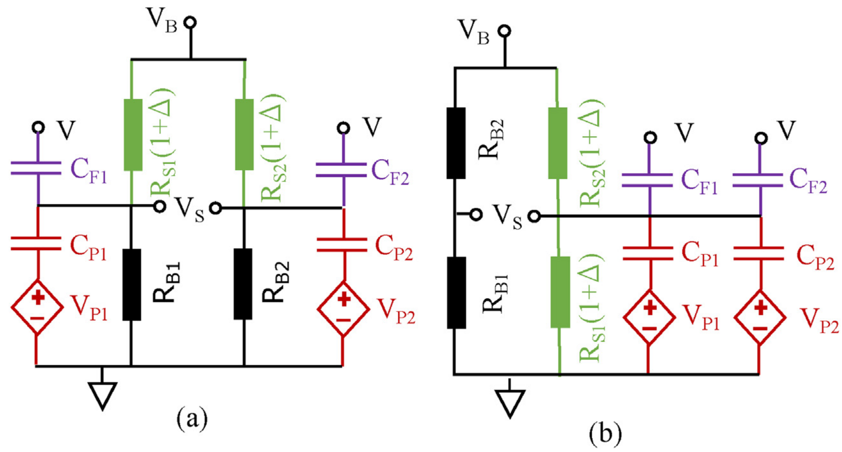

Fig. 2. Equivalent circuit diagram of Wheatstone Bridge. (a) Subtractive feedthrough configuration; (b) additive feedthrough configuration.

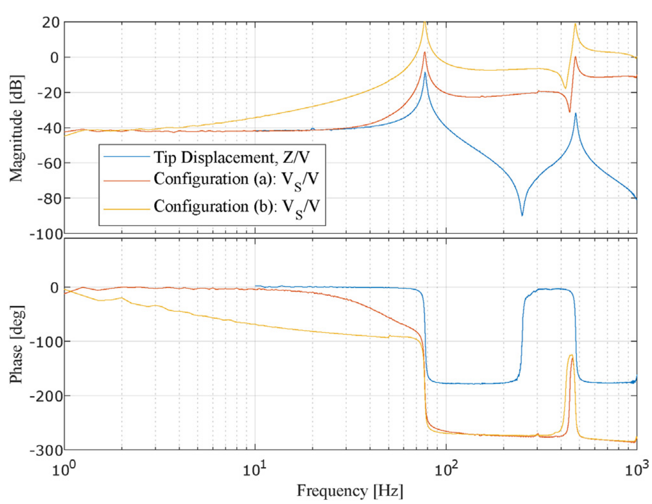

Fig. 3. Experimental frequency responses of the piezoelectric bender. Tip displacement over driving voltage (Z/V), and strain voltage over driving voltage (V_S/V) for configuration (a) and configuration (b) shown in Fig. 2.

strain response. This is slightly larger than half the first resonance frequency of the bender.

2.3. Quasi-static linear force model

Given the strain based measurement of deflection proposed in Section II, the electromechanical model of piezoelectric actuators [26] depicted in Fig. 4 provides a convenient way to estimate tip forces. The constitutive equations relating charge q, applied voltage, V, and applied force F to bender deflection, Z are given by:

$$m\ddot{Z} + b\dot{Z} + kZ = F + n(V - V_H) \tag{14}$$

$$q = nZ + C_P(V - V_H) \tag{15}$$

$$V_H = H(q) \tag{16}$$

where m, b, k, n and V_H represent equivalent moving mass, damping coefficient, stiffness, piezoelectric coupling factor, and hysteresis voltage respectively.

Eq. (14) is reformulated to provide a model for estimating tip force from the strain based position measurement Z and the voltage actuating the bender V:

$$F_{Model} = m\ddot{Z} + b\dot{Z} + kZ - n(V - V_H) \tag{17}$$

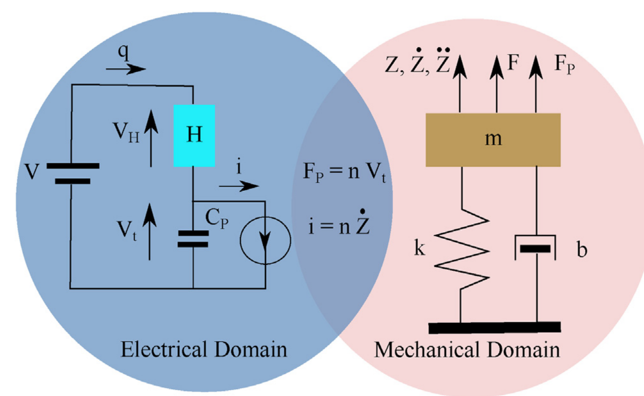

Fig. 4. Electromechanical model for piezoelectric actuators with hysteresis. The piezoelectric force F_P in the mechanical domain is coupled to the linear piezoelectric voltage V_t in the electrical domain through the piezoelectric coupling constant n. The difference between V_t and the actuating voltage V is attributed to the nonlinear hysteresis voltage V_H.

This model contains a nonlinear hysteresis voltage, V_H. Many hysteresis models are available to describe this relationship [7,8,27]. For simplicity, this article neglects higher order effects such as hysteresis, creep, friction, and inertia. This leads to a simple linear model for quasi-static applications:

$$F_{Model} = kZ - nV \tag{18}$$

The omission of hysteresis and creep are expected to result in force estimation errors of approximately 10%. The bandwidth of the force model is limited by the first resonance frequency of the bender itself (78 Hz), and the bandwidth of the strain measurement (44 Hz). For the bender in this study, the inertia terms in the force model are insignificant, since the force estimation bandwidth is dominated by the bandwidth of the strain measurement.

3. Experimental results

3.1. Experimental setup

The sensor performance is evaluated experimentally using the setup shown in Fig. 5. Reference tip displacement is measured with a Di-Soric LAT61 Laser triangulation sensor with a resolution of 1.5 μm and a bandwidth of 2.5 kHz. Reference forces are measured with a Forsentek FC10C-5kg strain based load cell with a maximum load rating of 5 kg. The load cell is mounted on a single axis positioning stage from Thorlabs to position the load cell relative to

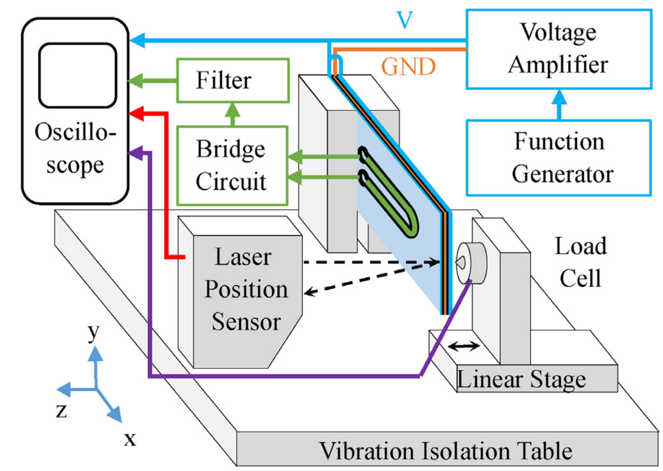

Fig. 5. Experimental setup. The bender is actuated through a function generator and a voltage amplifier. The strain gauges are connected to a bridge circuit and an anti-aliasing filter. A laser triangulation sensor and a load cell are employed as reference position and force sensors respectively.

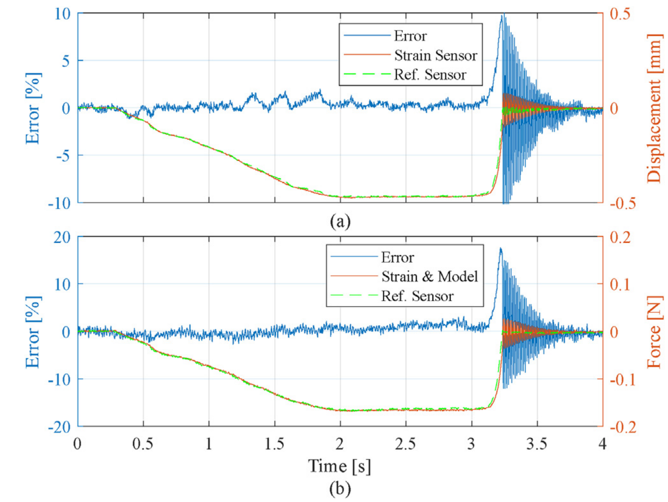

Fig. 6. Experimental strain gauge response of the piezoelectric bender due to a tip force. (a) Displacement and (b) force response.

the tip of the bender. The bender is excited by a 33522B Agilent Arbitrary Waveform Generator and a PiezoDrive PD200 amplifier. A custom bridge circuit with a 2.5 V bias voltage extracts strain measurements from the strain gauges integrated into the outside electrodes. A Krohn-Hite 3384 filter is used as an anti-aliasing filter and to adjust the gain of the strain measurements to 0.8 mm/V, identical to the reference position sensor. All measurements are recorded with a Tektronix TDS3034C Oscilloscope.

3.2. Compensation for elastic base clamping

The experimental resonant frequency in Fig. 3 is significantly lower than the manufacturer's specification in Table 1. This is an indication of a non-rigid clamping condition at the base of the bender. This was confirmed by experimentally obtaining the ratio of strain readings due to an actuating voltage $\frac{dS}{dZ}|_{F=0}$ to strain readings due to tip forces $\frac{dS}{dZ}|_{M_p=0}$.

$$G^* = \frac{\frac{dS}{dZ}|_{M_p=0}}{\frac{dS}{dZ}|_{F=0}} = 0.83, \tag{19}$$

Tip forces with the original strain gauge length of $2L/3$ underestimate the actual displacement by 17%, because the tip forces create bending moments and subsequent angular deflections at the base that are not present for applied voltages. Substituting Eqs. (4), (5), (8), (9), and (2) into Eq. (19) allows solving for base clamping stiffness:

$$\gamma = -\frac{12EIG^*}{3L(x_1+x_2)+L^2(4G^*-6)}, \tag{20}$$

Substituting Eq. (20) into Eq. (13), provides an expression for the required shortening of the strain gauges:

$$x_2^* = \frac{x_2}{G^*} + (2L - x_1)(1 - \frac{1}{G^*}) \tag{21}$$

This is implemented by adding a solder bridge across the strain gauge at $x_2^* = 22$ mm for the remaining experiments in this article.

3.3. Force excitation

In the experiment shown in Fig. 6, the bender is excited by slowly moving the load cell against the tip of the bender and then rapidly removing it towards the end of the experiment. During this experiment, zero actuation voltage is applied to the bender. Fig. 6 shows the displacement, force and the associated sensing errors as function of time. The position estimates from the strain readings exhibit errors smaller than 2% during the low frequency portion of the experiment. During the release of the bender, significant phase lag is developed that increases the sensing error to 10%. After release, lightly damped vibrations are observed that die out after 1 s. The vibrations are due to the lightly damped nature of the beam. The increase in sensing error is a result of the feedthrough components of V and V_P that become dominant at frequencies approaching the first resonance frequency as indicated in Fig. 3. A bender stiffness of $k = 0.35$ N/mm is obtained by fitting Eq. (18) to the reference force and reference displacement data. Substituting the fitted stiffness and the displacement obtained from the strain measurements back into Eq. (18), force fitting errors of less than 3% are observed during the low frequency loading portion of the experiment. During unloading, hysteresis and inertial forces become significant and force errors of up to 15% are observed.

3.4. Voltage excitation

In this experiment, the bender is actuated by a sinusoidal driving voltage with an amplitude of ±40 V and a frequency of 0.5 Hz. No tip force is applied in this experiment. Fig. 7 shows the displacement, force and the associated sensing errors as functions of time. Position errors less than 1.5% of the full scale displacement are recorded with no external forces present in Fig. 7a. A piezoelectric coupling factor of $n = 0.0035$ N/V is obtained by fitting Eq. (18) to the voltage excitation data using the stiffness obtained in the force excitation experiment. Force fitting errors of less than 6% are obtained. These are mainly caused by unmodelled hysteresis in Eq. (18).

3.5. Simultaneous voltage and force excitation

In the last experiment, the bender is driven into the stationary load cell using a 0.5 Hz sinusoidal voltage with an amplitude of 40 V. The experimental response plotted in Fig. 8a indicates that the positions identified from the strain sensor are accurate to within 2.5% even for significant blocking forces. The simple linear force model in Fig. 8b shows modeling errors of up to 8% that could be reduced with hysteresis and creep models.

Table 2
Bender sensing errors.

	Proposed system	Mansour 2018 [23]	Ballas 2007 [18]	Ballas 2007 [18]	Ronkanen 2007 [28]	Rakotondrabe 2015 [12]
Displacementsensing						
Measurement principle	Strain	Strain	Capacitive strain	Inductive proximity	–	Model (V)
Measurement range	900 μm	2000 μm	300 μm	300 μm	–	3.1 μm
Measurement bandwidth	44 Hz	10 Hz	Static	1 kHz		Quasi static
Force excitation error	2%	–	–	–	–	–
Voltage excitation error	1.5%	1.1%	5.9%	4.8%	–	–
Force and voltage excitation error	2.5%	–	–	–	–	6.5%
Forcesensing						
Measurement principle	Model (S,V)	–	–	–	Model (Z,V,I)	Model (V)
Measurement range	230 mN	–	–	–	90 mN	1.15 mN
Measurement bandwidth	44 Hz	–	–	–	Static	Quasi static
Force excitation error	3%	–	–	–	9%	–
Voltage excitation error	6%	–	–	–	–	–
Force and voltage excitation error	8%	–	–	–	–	4.3%

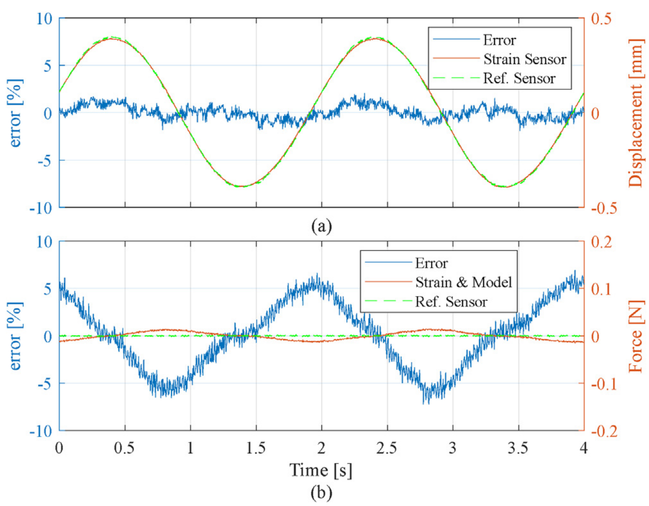

Fig. 7. Experimental strain gauge response of the piezoelectric bender due to a sinusoidal driving voltage. (a) Displacement and (b) force response.

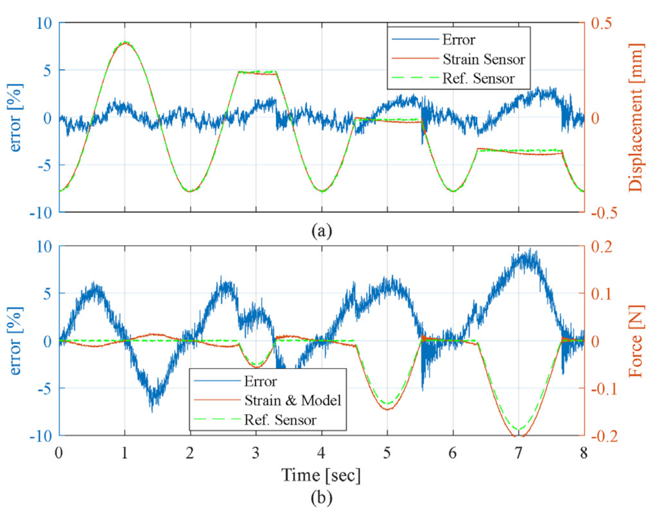

Fig. 8. Experimental strain gauge response of the piezoelectric bender due to a sinusoidal driving voltage and hard stops at three different positions. (a) Displacement and (b) force response.

3.6. Comparison with the state of the art

The majority of research on measuring bender deflection neglects tip forces. The work that includes the interaction between force and deflection often shows incomplete or no data on sensing errors. Table 2 compares the little quantitative data that we were able to compile from other works. These include integrated strain, capacitive and inductive sensing techniques, as well as two modeling techniques.

The proposed system's displacement measurement errors of less than 2.5% compare well with previous strain based measurements showing 1.1% error [23] and capacitive and inductive measurement techniques with errors of 5.9% and 4.8% respectively [18]. The presented results are particularly impressive, since they consider significant tip forces for the first time. The bandwidth of the proposed sensing system only lags behind the inductive proximity sensor [18]. However, the proximity sensor is is not truly integrated into the electrode since it requires an external pickup coil.

No integrated force sensors are reported in the literature. Thus, the proposed system's force measurements are compared to model based approaches. A neural network model linking tip force to a measurement of displacement, actuating voltage, and driving current [28] shows slightly larger force estimation errors than the proposed system. In addition, it requires an external position sensor. Another approach uses a specialized measuring circuit and a dynamic observer to estimate both tip force and displacement [12] of benders. This technique provides lower force error magnitudes, but its position sensing is less accurate and the reported validation experiments are quasi static.

4. Conclusions

In this article, a design procedure for integrating strain gauges into the electrodes of piezoelectric bending actuators with the aim of measuring tip deflections is proposed. The main novelty of the design is the ability to measure tip displacements induced by two simultaneous excitation sources: actuating voltages and external tip forces. The sensing technique is validated experimentally and displacement sensing errors of less than 2.5% are consistently achieved for different operating conditions. The bandwidth of the sensor is close to half the first resonance frequency of the bender. A simple linear model is also presented to augment the position measurements with estimates of the tip forces acting on the bender. This model displays less than 8% force estimation error. The authors are currently working on the evaluation of the sensor at different temperatures and the integration into position control applications.

Declaration of interests

None.

Authors' contribution

R.J. Seethaler: Conceptualization, Methodology, Investigation, Writing – Original draft preparation, Visualization; S.Z. Mansour: Conceptualization, Writing – Reviewing and Editing; M.G. Ruppert: Conceptualization, Methodology, Validation, Writing – Reviewing and Editing, Visualization; A.J. Fleming: Conceptualization, Resources, Writing – Reviewing and Editing, Visualization.

Declaration of Competing Interest

The authors report no declarations of interest.

References

[1] P. Smithmaitrie, J. Kanjantoe, P. Tandayya, Touching force response of the piezoelectric Braille cell, Disabil. Rehabil. Assist. Technol. 3 (6) (2008) 360–365, http://dx.doi.org/10.1080/17483100802281442.
[2] K. Mista, Warp Knitting Machine with Jacquard-Control (1993). https://patents.google.com/patent/EP0583631A1/en.
[3] H.J. Ramsey, M.L. Dakss, Piezoelectric Optical Switch (1979). https://patents.google.com/patent/US4303302/en.
[4] K.W. Chan, W.-h. Liao, Precision positioning of hard disk drives using piezoelectric actuators with passive damping, 2006 International Conference on Mechatronics and Automation (2006) 1269–1274, http://dx.doi.org/10.1109/ICMA.2006.257809, ISSN: 2152-744X.
[5] White Paper Piezo Technology in Pneumatic Valves, Tech. Rep., Festo AG & Co KG (2017).
[6] F. Giessibl, Atomic Resolution of the Silicon (111)-(7x7) Surface by Atomic Force Microscopy, Science (New York, N.Y.) 267 (1995) 68–71, http://dx.doi.org/10.1126/science.267.5194.68.
[7] B. Mokaberi, A.A. Requicha, Compensation of scanner creep and hysteresis for afm nanomanipulation, IEEE Trans. Autom. Sci. Eng. 5 (2) (2008) 197–206.
[8] M. Rakotondrabe, Bouc-Wen modeling and inverse multiplicative structure to compensate hysteresis nonlinearity in piezoelectric actuators, IEEE Trans. Autom. Sci. Eng. 8 (2) (2011) 428–431, http://dx.doi.org/10.1109/TASE.2010.2081979.
[9] K. Furutani, M. Urushibata, N. Mohri, Improvement of control method for piezoelectric actuator by combining induced charge feedback with inverse transfer function compensation, Proceedings of the 1998 IEEE International Conference on Robotics and Automation, vol. 2 (1998) 1504–1509, http://dx.doi.org/10.1109/ROBOT.1998.677325.
[10] A.J. Fleming, S.O.R. Moheimani, A grounded-load charge amplifier for reducing hysteresis in piezoelectric tube scanners, Rev. Sci. Instrum. 76 (2005) 073707, http://dx.doi.org/10.1063/1.1938952.
[11] M.G. Ruppert, S.R. Moheimani, High-bandwidth multimode self-sensing in bimodal atomic force microscopy, Beilstein J. Nanotechnol. 7 (1) (2016) 284–295.
[12] M. Rakotondrabe, I.A. Ivan, S. Khadraoui, P. Lutz, N. Chaillet, Simultaneous displacement/force self-sensing in piezoelectric actuators and applications to robust control, IEEE/ASME Trans. Mechatron. 20 (2) (2015) 519–531, http://dx.doi.org/10.1109/TMECH.2014.2300333.
[13] M.N. Islam, R.J. Seethaler, Sensorless Position control for piezoelectric actuators using a hybrid position observer, IEEE/ASME Trans. Mechatron. 19 (2) (2014) 667–675, http://dx.doi.org/10.1109/TMECH.2013.2250990.
[14] F. Arai, A. Kawaji, T. Sugiyama, Y. Onomura, M. Ogawa, T. Fukuda, H. Iwata, K. Itoigawa, 3D micromanipulation system under microscope, MHA'98. Proceedings of the 1998 International Symposium on Micromechatronics and Human Science (1998) 127–134, http://dx.doi.org/10.1109/MHS.1998.745764.
[15] A. Menciassi, A. Eisinberg, M. Carrozza, P. Dario, Force sensing microinstrument for measuring tissue properties and pulse in microsurgery, IEEE/ASME Trans. Mechatron. 8 (1) (2003) 10–17, http://dx.doi.org/10.1109/TMECH.2003.809153.
[16] M. Goldfarb, N. Celanovic, A flexure-based gripper for small-scale manipulation, Robotica 17 (2) (1999) 181–187, http://dx.doi.org/10.1017/S026357479900096X.
[17] D. Campolo, R. Sahai, R. Fearing, Development of piezoelectric bending actuators with embedded piezoelectric sensors for micromechanical flapping mechanisms, IEEE International Conference on Robotics and Automation, vol. 3 (2003) 3339–3346, http://dx.doi.org/10.1109/ROBOT.2003.1242106.
[18] R.G. Ballas, Piezoelectric Multilayer Beam Bending Actuators: Static and Dynamic Behavior and Aspects of Sensor Integration, Microtechnology and MEMS, Springer-Verlag, Berlin Heidelberg, 2007, http://dx.doi.org/10.1007/978-3-540-32642-7 https://www.springer.com/gp/book/9783540326410.
[19] M.G. Ruppert, S.O.R. Moheimani, A novel self-sensing technique for tapping-mode atomic force microscopy, Rev. Sci. Instrum. 84 (12) (2013) 125006.
[20] M.G. Ruppert, S.I. Moore, M. Zawierta, A.J. Fleming, G. Putrino, Y.K. Yong, Multimodal atomic force microscopy with optimized higher eigenmode sensitivity using on-chip piezoelectric actuation and sensing, Nanotechnology 30 (8) (2019) 085503.
[21] M.G. Ruppert, A.G. Fowler, M. Maroufi, S.R. Moheimani, On-chip dynamic mode atomic force microscopy: a silicon-on-insulator mems approach, IEEE J. Microelectromech. Syst. 26 (1) (2017) 215–225.
[22] P. Rougeot, A. Mohand-Ousaid, D. Gendreau, M. Hammouche, M. Rakotondrabe, Design, modeling and simulation of a three-layer piezoelectric cantilevered actuator with collocated sensor, Sensors for Next-Generation Robotics III, vol. 9859 (2016) 98590F.
[23] S. Zarif Mansour, R.J. Seethaler, Y.R. Teo, Y.K. Yong, A.J. Fleming, Piezoelectric bimorph actuator with integrated strain sensing electrodes, IEEE Sens. J. 18 (14) (2018) 5812–5817, http://dx.doi.org/10.1109/JSEN.2018.2842138.
[24] F. Beer, E. Johnson, J. deWolf, D. Mazurek, Mechanics of Materials, McGraw Hill, 2006.
[25] R.B. Northrop, Introduction to Instrumentation and Measurements, CRC Press, 2005.
[26] M. Goldfarb, N. Celanovic, A lumped parameter electromechanical model for describing the nonlinear behavior of piezoelectric actuators, J. Dyn. Syst. Meas. Control 119 (3) (1997) 478–485, http://dx.doi.org/10.1115/1.2801282.
[27] S.Z. Mansour, R. Seethaler, A. Fleming, A simple asymmetric hysteresis model for displacement-force control of piezoelectric actuators, 2018 IEEE/ASME International Conference on Advanced Intelligent Mechatronics (AIM) (2018) 87–90, http://dx.doi.org/10.1109/AIM.2018.8452221.
[28] P. Ronkanen, P. Kallio, H.N. Koivo, Simultaneous actuation and force estimation using piezoelectric actuators, 2007 International Conference on Mechatronics and Automation (2007) 3261–3265, http://dx.doi.org/10.1109/ICMA.2007.4304084.

Biographies

Rudolf J. Seethaler (M'07) received the B.Sc. degree in mechanical engineering at the University of Toronto, Canada, in 1991 and the Ph.D. degree in mechanical engineering from the University of British Columbia (UBC), Vancouver, BC, Canada, in 1997. From 1997 to 2005, he was a Senior Controls Engineer at BMW AG, Munich, Germany. He is currently an Associate Professor with UBC. His research interests include the design and control of high-speed motion control systems, and the optimization of manufacturing processes.

Sepehr Zarif Mansour received the Bachelor's of Applied Science degree in mechanical engineering from the University of Tehran, Tehran, Iran, in 2013, and the PhD degree in mechanical engineering with the University of British Columbia, Kelowna, BC, Canada, in 2019. He is currently working at York University, Toronto, Canada as a postdoctoral research fellow. His research interests include the design and control of high-speed motion control systems.

Michael G. Ruppert received the Dipl.-Ing. degree in automation technology from the University of Stuttgart, Germany, in 2013 and the PhD degree in Electrical Engineering from The University of Newcastle, Australia in 2017. As a visiting researcher, he was with The University of Texas at Dallas, USA from 2015 until 2016 and he is currently a postdoctoral research fellow at The University of Newcastle. His research interests include the utilization of system theoretic tools for sensing, estimation and control in high-speed and multifrequency atomic force microscopy. Dr Ruppert's research has been recognized with the 2019 Best Conference Paper Award at the 2019 International Conference on Manipulation, Automation and Robotics at Small Scales (MARSS), the 2018 IEEE Transactions on Control Systems Technology Outstanding Paper Award, and the 2017 University of Newcastle Higher Degree by Research Excellence Award.

Andrew J. Fleming (M'02) received the B.Sc. degree in electrical engineering and the Ph.D. degree in mechatronics engineering from the University of New-castle, Callaghan, NSW, Australia, in 2000 and 2004, respectively. He is currently an Australian Research Council Future Fellow and the Director with the Precision Mechatronics Lab, University of Newcastle. He is the co-author of three books, and more than 180 journal and conference articles. He is the Inventor of several patent applications. His research interests include lithography, nano positioning, scanning probe microscopy, and biomedical devices. Dr. Fleming received the Academy for Technological Sciences and Engineering Baterham Medal in 2016, the Newcastle Innovation Rising Star Award for Excellence in Industrial Engagement in 2012, the IEEE Control Systems Society Outstanding Paper Award in 2007, and the University of Newcastle Researcher of the Year Award in 2007.